TABLE 1

*Summary of characteristics in 11 cases of opercular glioma**

Case No.	Age (yrs), Sex	Diagnosis	WHO Grade	Tumor Location	Dominant Hemisphere	Presenting Symptoms	Date of Surgery	State of Anesthesia
1	26, M	A	II	rt face motor area	no	lt facial seizure followed by generalized convulsion	1/23/97	awake
2	31, M	AA	III	lt face/tongue motor area	yes	generalized convulsion	9/11/97	awake
3	68, M	AA	III	rt tongue sensorimotor area	no	lt facial seizure	1/27/98	awake
4	3, M	DNET	I	rt face motor area	no	lt facial seizure	12/16/99	general
5	38, M	AA	III	lt face motor area	yes	lt facial seizure	2/28/00	general
6	69, F	GBM	IV	rt face/tongue sensorimotor area	no	lt facial seizure followed by lt hemiconvulsion	1/24/02	general
7	49, M	OA	II	rt tongue sensorimotor area	no	incidental	2/5/02	general
8	21, M	A	II	lt tongue sensorimotor area	no	rt facial seizure followed by generalized convulsion	4/11/02	general
9	38, M	AA	III	rt face motor area	no	lt facial seizure	7/22/02	general
10	34, F	O	II	lt face/tongue motor area	yes	rt facial seizure	4/28/03	awake
11	23, M	AA	III	lt face motor area	yes	loss of consciousness	6/9/05	awake

* A = astrocytoma; AA = anaplastic astrocytoma; DCS = direct cortical stimulation; DNET = dysembryoplastic neuroepithelial tumor; KPS = Karnofsky Performance Scale; O = oligodendroglioma; OA = oligoastrocytoma; SCS = subcortical stimulation; US = ultrasonography; WHO = World Health Organization.

Clinical Material and Methods

Patient Population and Tumor Characteristics

This study included 11 consecutive patients, nine males and two females with ages from 3 to 69 years (mean 36.4 ± 19.8 years). Each patient harbored a newly diagnosed glioma located at the opercular region around the orofacial primary motor and somatosensory cortices but not involving either the hand/digit area or the insula and treated in our department after 1997. The tumors included one dysembryoplastic neuroepithelial tumor, two astrocytomas, one oligoastrocytoma, one oligodendroglioma, five anaplastic astrocytomas, and one GBM. Patient characteristics are summarized in Table 1. Informed consent for this study was obtained from all the patients, and institutional review board approval was waived because of the retrospective nature of the study.

Surgical Procedure and Intraoperative Neurophysiological Monitoring

All patients underwent open surgery for maximum tumor resection. Cortical mapping was performed in eight patients, using electric stimuli of 3 to 12 mA to identify the sensorimotor and language cortices, according to a method described previously.[1-4] Five patients were treated while in an awake condition. Primary speech cortex was identified based on speech arrest or hesitation due to stimulation during counting or object naming by the patient. A frameless stereotactic navigation device (ISG Viewing Wand, ISG Technologies; ViewScope, Elekta IGS; or Vector Vision, BrainLAB) was used in all nine cases after 1998; ultrasonography was used in the initial two cases.

Tumor resection was performed using an Ultrasonic Surgical Aspirator (Sonopet, Miwatec Co., Ltd.). All of the opercular arteries were carefully dissected and preserved. If the tumor infiltrated down to the sylvian fissure, thorough dissection of the affected sylvian fissure was initially performed to identify and preserve the insular and opercular segments of the MCAs.

Only the minimum amount of Surgicel (Ethicon, Inc.) was routinely used for hemostasis. Dexamethasone (4 mg) was given every 6 hours with varied tapering schedules, and the administration of anticonvulsants (typically phenytoin and/or zonisamide) and antibiotics was begun or continued in patients during the immediate postoperative period.

Neuroimaging Studies

All patients underwent preoperative, postoperative, and subsequent follow-up MR imaging at our department. Postoperative imaging was performed within 72 hours of surgery. Data from pre- and postoperative DW MR imaging were available for the nine consecutive patients treated after 1998.

For MR imaging, we used a 1.5-tesla system (Signa Horizon LX CV/i, GE Medical Systems) with a conventional quadrature head coil. We obtained T_1-weighted images before and after Gd administration, T_2-weighted images, and DW images during the same imaging session without repositioning the patient's head. Axial DW images were obtained using fat-suppressed spin echo–echo planar imaging (TR 5000 msec, TE 72 msec, number of excitations 2, slice thickness 6 mm, gap 2 mm, matrix 128 × 128, and field of view 23 × 23 cm) with three orthogonal directional motion-probing gradients (b = 1000 seconds/mm^2), followed by automatic generation of isotropic DW images. To evaluate the

TABLE 1
(continued)

Stimulation	Navigation System	Extent of Resection	DW Image	Immediate Postop Outcome	Long-Term Deficit	Follow Up (3/26/06)
DCS	US	total	not examined	lt facial palsy	none	no recurrence, KPS 100
DCS	US	total	not examined	rt facial palsy, dysarthria	slight dysarthria	no recurrence, KPS 90
DCS	viewing wand	total	infarction beneath resection cavity	lt hemiparesis	lt fine movement disorder	dead 5/14/99 (dissemination)
none	ViewScope	total	infarction beneath resection cavity	lt hemiparesis	none	no recurrence, KPS 100
DCS & SCS	ViewScope	total	infarction beneath resection cavity	rt facial palsy, dysarthria	slight dysarthria	no recurrence, KPS 90
DCS & SCS	ViewScope	subtotal	infarction beneath resection cavity	lt hemiparesis	lt hemiparesis	dead 4/28/04 (local recurrence & dissemination)
none	ViewScope	total	infarction beneath resection cavity	lt facial palsy	none	no recurrence, KPS 100
none	ViewScope	total	infarction beneath resection cavity	none	none	no recurrence, KPS 100
DCS & SCS	ViewScope	total	infarction beneath resection cavity	none	none	no recurrence, KPS 100
DCS & SCS	ViewScope	subtotal	infarction beneath resection cavity	rt facial palsy, dysarthria	dysarthria	no recurrence, KPS 90
DCS & SCS	Vector Vision	subtotal	infarction beneath resection cavity	rt fine movement disorder, dysarthria	none	no recurrence, KPS 100

spatial relationship between the postoperative ischemic lesion and the pyramidal tract, coronal DW images were also obtained using similar conditions, but the motion-probing gradient was applied in only the anteroposterior direction. The pyramidal tracts, which run in the cephalocaudal direction, were delineated as slightly hyperintense to adjacent brain parenchyma in these coronal images.

The extent of the resection was evaluated according to MR images obtained within 72 hours of surgery. If the tumor had been enhanced on the preoperative MR images, its gross-total resection was defined as no residual enhanced tumor, its subtotal resection as more than 75% removal, and its partial resection as less than 75% removal. If the tumor had not been enhanced on the preoperative MR images, resection was evaluated based on the presence of residual high-intensity lesion on the T_2-weighted MR images.

Postoperative Neurological Outcomes

The postoperative neurological outcome was recorded and confirmed by retrospective review of all hospital records and physician notes. Immediate postoperative neurological function was determined during the first 7 days after surgery, and long-term function was determined between 3 and 6 months after surgery.

Microangiographic Analysis of Vascular Supply to the Corona Radiata

Coronal and axial microangiograms of five cadaveric brains without gross brain pathological features, which were part of a microangiographic study on the distribution of the basal perforating arteries that had been conducted by one of the authors (S.T.) in 1985,[17,18] were reanalyzed to examine pial cortical arteries in and around the insuloopercular region and to identify the blood supply to the corona radiata.

Results

Extent of Resection

Table 1 outlines the extent of resection in each case, as determined by quantitative volumetric analysis using postoperative MR imaging. Gross-total resection of the lesions was accomplished in eight patients (Cases 1–5 and 7–9). Subtotal resection was achieved in three patients (Cases 6, 10, and 11).

Postoperative MR Imaging and Neurological Outcomes

Postoperative DW MR images showed markedly hyperintense areas representing restricted diffusion in all nine patients treated after 1998. These lesions were all contiguous with the resection cavity. The size of the lesions beneath the resection cavity varied from case to case. All lesions appeared as high-intensity areas on T_2-weighted MR images. Similar high-intensity lesions were also depicted on postoperative T_2-weighted images in the two initial patients without DW imaging data.

Details on postoperative neurological deficits are shown in Table 1. Eight patients, all of whom had undergone relatively small areas of resection mostly located in the face motor area, did not suffer impairment of long-tract function after surgery; three patients (Cases 3, 4, and 6) did have impaired long-tract function immediately after surgery. The lesions with restricted diffusion involved the descending motor pathway in these three patients. Tumor was located in the orofacial sensorimotor area in two of these patients

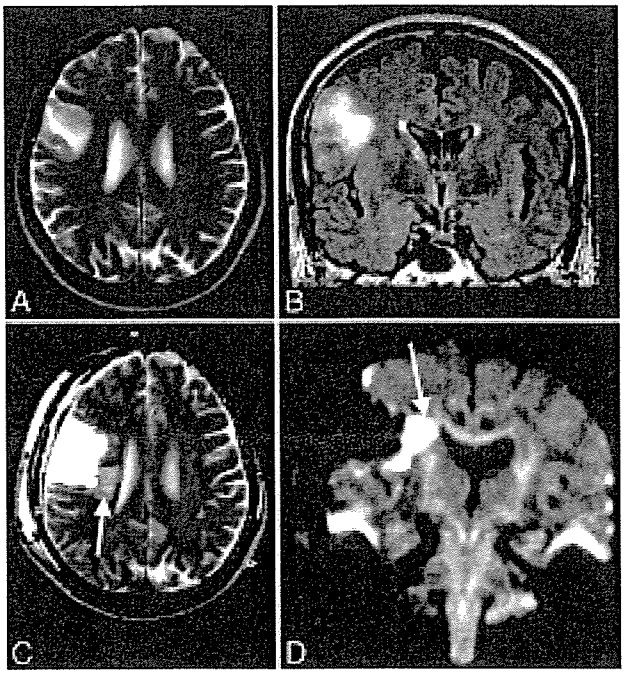

FIG. 1. Case 3. Images obtained in a 68-year-old man with an anaplastic astrocytoma in the right tongue sensorimotor area. Preoperative axial T_2-weighted (A) and coronal fluid-attenuated inversion-recovery (B) MR images revealing a high-intensity mass in the right frontoparietal opercular region. Postoperative axial T_2-weighted (C) and coronal DW (D) MR images showing total removal of the tumor and a new high-intensity lesion *(arrows)* beneath the resection cavity. The lesion extends to the region of the corona radiata, probably involving the corticospinal tract. This tract appears as a bandlike area of slightly high intensity on the coronal DW image with the motion-probing gradient applied only in the anteroposterior direction.

(Cases 3 and 6). A relatively small resection in these two patients was performed around the white matter above the upper limiting sulcus of the posterior region of the insula, and wide resection was undertaken in the anteroposterior and cephalocaudal directions of the opercular region (Figs. 1–4).

Microangiographic Analysis of Vascular Supply to the Corona Radiata

Coronal microangiography of the cadavers showed that the corona radiata is constantly supplied by the lateral striate arteries, the long insular arteries originating from insular portions of the MCA, and the medullary arteries from the opercular and cortical portions of the MCA (Fig. 5). Surgical removal for opercular glioma, even if not involving the insula, could compromise the latter two fine arteries, resulting in cerebral infarction at the corona radiata.

Illustrative Cases

Case 3

History and Examination. This 68-year-old man presented with an anaplastic astrocytoma manifesting as left facial seizures. Results of T_2-weighted MR imaging demonstrated a hyperintense lesion in the right opercular portions of the inferior frontal, precentral, and postcentral gyri inferolateral to the precentral knob, not involving the insula (Fig. 1A). Administration of a contrast medium caused no enhancement. Neurological and neuropsychological examination revealed no abnormality.

Operation. A right frontoparietotemporal craniotomy was performed with the patient in an awake condition. Direct cortical stimulation identified the face motor area and the primary sensory sites of the tongue and face. The sylvian fissure was thoroughly dissected toward the distal end, and the insular surface was exposed under the operating microscope. The precentral and central arteries were separated from the tumor and preserved. The lesion was totally removed up to the face motor area and toward the deepest portion using the upper limiting sulcus as the anatomical landmark and the ISG Viewing Wand (Fig. 2).

Postoperative Course. Almost complete left hemiparesis was observed postoperatively. Magnetic resonance images showed that the entire lesion had been resected but revealed an ischemic area beneath the resection cavity involving the descending motor pathway (Fig. 1B). As adjuvant therapy, the patient received 72 Gy hyperfractionated radiation to the extended local field. His left hemiparesis resolved except

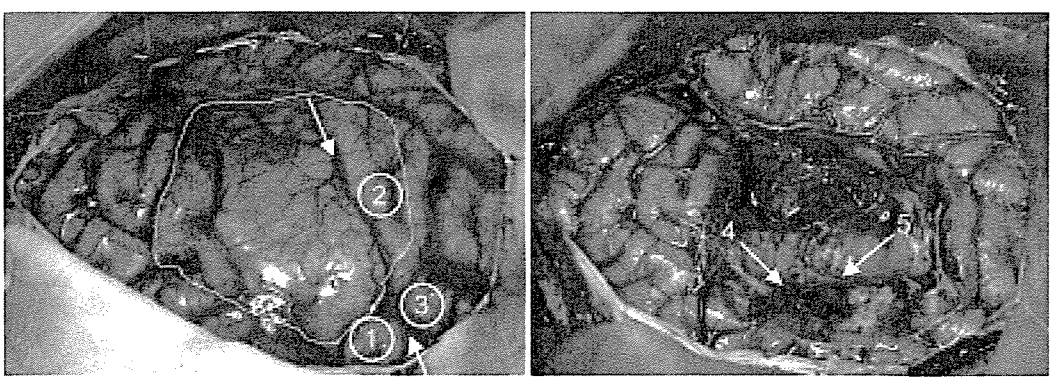

FIG. 2. Case 3. Intraoperative photographs obtained before *(left)* and after *(right)* tumor resection. *Left:* Note the results of functional brain mapping: 1, face motor; 2, tongue sensory; and 3, face sensory. The outline indicates the location of the tumor; the *arrows* represent the central sulcus. *Right:* Note preservation of the precentral (4) and central (5) arteries.

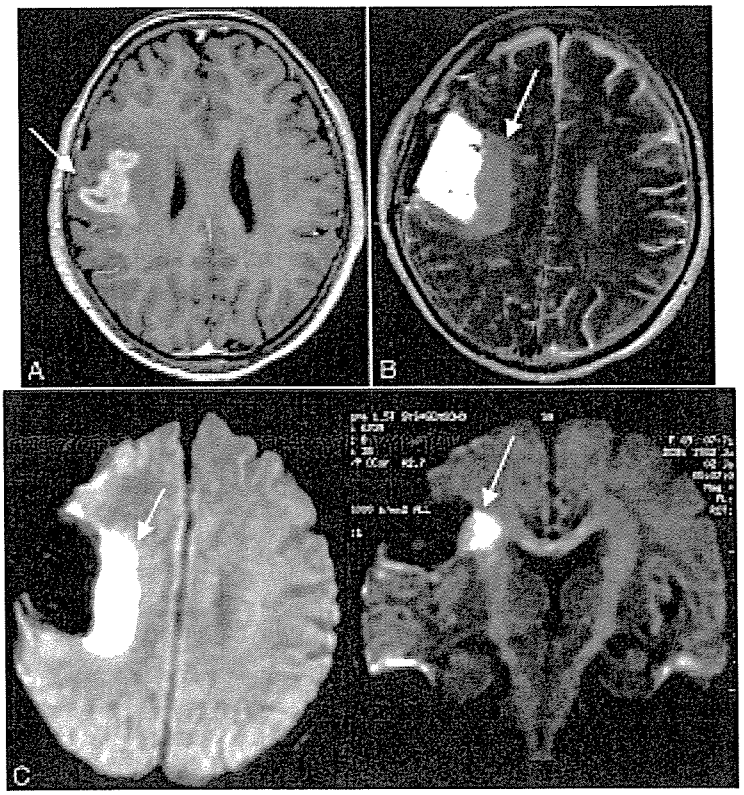

FIG. 3. Case 6. Images obtained in a 69-year-old woman with a right frontoparietal GBM. A: Preoperative axial Gd-enhanced T_1-weighted MR image demonstrating an irregularly enhanced mass lesion in the opercular region around the central sulcus *(arrow)*. B: Postoperative axial T_2-weighted MR image depicting total removal of the tumor and a new lesion of high intensity *(arrow)* beneath the resection cavity. C: Postoperative axial *(left)* and coronal *(right)* DW MR images revealing the new lesion *(arrows)* beneath the resection cavity with reduced diffusion probably involving the corticospinal tract.

for impaired fine movement of the left finger. He was discharged home and able to ambulate 2 months postsurgery.

Case 6

History and Examination. This 69-year-old woman presented with a GBM manifesting as left facial seizures followed by left hemiconvulsion. Preoperative T_1-weighted MR images with contrast medium exhibited an enhanced mass in the right opercular portions of the inferior frontal, precentral, and postcentral gyri inferolateral to the precentral knob, not involving the insula (Fig. 3A). Neurological and neuropsychological examination revealed no abnormality.

Operation. A right frontoparietotemporal craniotomy was performed with the patient in a state of general anesthesia. Direct cortical stimulation identified the hand/digit motor area. The sylvian fissure was thoroughly dissected toward the distal end, and the insular surface was exposed under the operating microscope. The precentral, central, and anterior parietal arteries were separated from the tumor and preserved. The lower portion of the lesion was resected toward the deepest portion by using the upper limiting sulcus as the anatomical landmark and the ViewScope. The tumor was removed in a stepwise manner while monitoring the muscle contraction by direct cortical stimulation to the hand/digit motor area (Fig. 4). The positive cortical response gradually became duller at the end of the surgery.

Postoperative Course. Almost complete left hemiparesis was observed postoperatively. Magnetic resonance images obtained after surgery showed that most of the enhanced lesion had been resected, but an ischemic area was found beneath the resection cavity involving the descending motor pathway (Fig. 3B and C). The patient's left hemiparesis did not resolve.

Discussion

Surgical removal of glioma in the opercular region presents many challenges. In 1991, LeRoux et al.[11] first reported that gliomas involving the nondominant face motor cortex can be safely removed using brain mapping techniques to localize the rolandic cortex and avoid resection of the hand motor cortex and descending subcortical motor pathways. However, resection of the face motor cortex in the dominant hemisphere was not recommended because language localization in the cortical zones is contiguous with this region. In 1995, Ebeling and Kothbauer[5] supposed that radical tumor resection of a purely opercular glioma, not including the insula, in the dominant hemisphere can be

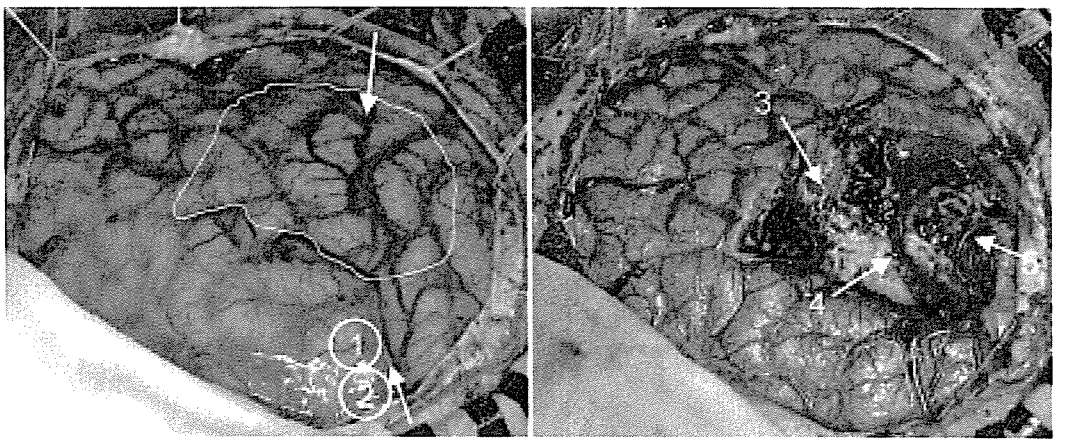

FIG. 4. Case 6. Intraoperative photographs obtained before *(left)* and after *(right)* tumor resection. *Left:* Note the results of functional brain mapping: 1 and 2, hand/digit motor. The *outline* indicates the tumor location; the *arrows* represent the central sulcus. *Right:* Note preservation of the precentral (3), central (4), and anterior parietal (5) arteries.

achieved without significant lasting morbidity. However, only biopsy was recommended for large dominant insular or opercular–insular tumors, because the lenticulostriate arteries hinder total resection and no clear border toward the internal capsule can be found. In 2004, Peraud et al.[12] reported the surgical results of 14 cases of opercular gliomas, stressing the importance of intraoperative neuromonitoring as an aid to surgery in the dominant opercular region. The severity and duration of postoperative deficits was well correlated with the distance from the resection margin to the next positive stimulation point(s), and a distance of more than 5 mm was found to avoid major impairments. Clearly, intraoperative functional brain mapping techniques can help preserve cortical and subcortical functions. However, vascular damage during resection of opercular glioma remains less well understood.

Recently, restricted diffusion abnormalities were found adjacent to the resection cavity on immediately postoperative images in 64% of cases.[15] Both cortical and subcortical lesions with restricted diffusion were observed after surgery. In the present study, postoperative MR images including DW images disclosed infarcted lesions in all patients, and these lesions unexpectedly extended to the descending motor pathway in the corona radiata in three patients, which could have resulted in the impairment of long-tract function. These infarcted lesions were probably caused by disruption of the blood supply during the surgical procedures.

Microangiographic analysis in this study revealed that the corona radiata is supplied by the lateral striate arteries, long insular arteries, and medullary arteries from the opercular and cortical segments of the MCA passing over the frontoparietal operculum. According to the study data collected by Ture et al.,[20] approximately 85 to 90% of insular arteries are short and supply the insular cortex and extreme capsule, 10% are medium length and supply the claustrum and external capsule, and 3 to 5% are long and extend as far

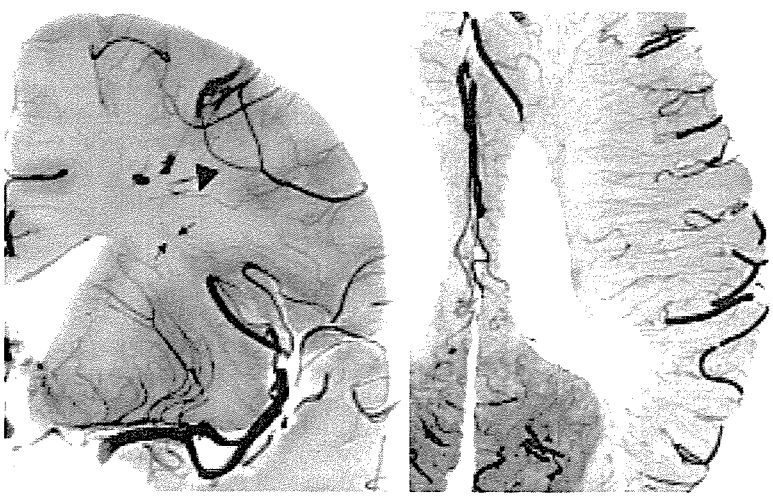

FIG. 5. Coronal *(left)* and axial *(right)* microangiograms of a cadaveric brain slice through the interventricular foramina. Both long insular arteries *(arrows)* arising from the insular portions of the MCA and the medullary arteries *(arrowhead)* from the opercular and cortical portions of the MCA course toward the ventricular wall and supply the region of the corona radiata.

as the corona radiata. Interruption of blood flow to these long insular arteries during the resection of intrinsic insular tumor may result in hemiparesis; thus, these arteries should be preserved to prevent infarction of the corona radiata.[6,10,19,20]

Data in the present study demonstrated that, in addition to the long insular arteries, the long medullary arteries from the opercular and cortical segments of the MCA passing over the frontoparietal operculum contribute to the arterial supply to the corona radiata. Although the vascular supply can show individual variations, these long medullary arteries can be impaired during the resection of a pure opercular glioma. Adequate collateral blood supply would not be expected[13] because intraparenchymal arterioles such as the lateral striate arteries, long insular arteries, and long medullary arteries are all end arteries without substantial anastomoses with other arteries except in pathological cases like moyamoya disease. If the impaired arteries supply most of the descending motor pathway, resection of opercular glioma is likely to result in hemiparesis.

The long insular arteries are mostly located in the posterior region of the insula,[20] most commonly on the posterior half of the central insular sulcus and on the long gyri.[19] Thus, subcortical resection around the upper limiting sulcus of the posterior region of the insula carries a higher risk of sacrifice of the long insular arteries, which may lead to extensive corona radiata infarction, and ultimately critical damage to the descending motor pathway. Similarly, a wide resection in the anteroposterior and cephalocaudal directions of the opercular region could damage a large number of medullary arteries from the opercular and cortical segments of the MCA over the frontoparietal operculum. In our experience, these two maneuvers appeared to be risk factors for critical infarction in the corona radiata after resection of an opercular glioma. However, reliable methods for avoiding damage to the long insular and medullary arteries are not available. Limited resection of the operculum as well as sparing of the posterior region of the insula may be the only measures presently available to avoid injury to a large number of long insular arteries and long medullary arteries. The development of new surgical devices to remove an opercular glioma with preservation of thin blood vessels like these arteries is to be expected in the future.

Conclusions

In the present study we found that ischemic complications occurring beneath the resection cavity including the pyramidal tract within the corona radiata are caused by damage to the distributing arteries—in particular, the long insular arteries and/or medullary arteries from the opercular and cortical segments of the MCA passing over the frontoparietal operculum—after resection of glioma in the frontoparietal opercular region inferolateral to the hand/digit sensorimotor area. Surgeons should be aware of the risk of ischemic complications during resection of opercular glioma and the possibility of permanent motor deficits.

References

1. Berger MS: Malignant astrocytomas: surgical aspects. **Semin Oncol 21:**172–185, 1994
2. Berger MS, Deliganis AV, Dobbins J, Keles GE: The effect of extent of resection on recurrence in patients with low grade cerebral hemisphere gliomas. **Cancer 74:**1784–1791, 1994
3. Berger MS, Kincaid J, Ojemann GA, Lettich E: Brain mapping techniques to maximize resection, safety, and seizure control in children with brain tumors. **Neurosurgery 25:**786–792, 1989
4. Berger MS, Ojemann GA, Lettich E: Neurophysiological monitoring during astrocytoma surgery. **Neurosurg Clin N Am 1:** 65–80, 1990
5. Ebeling U, Kothbauer K: Circumscribed low grade astrocytomas in the dominant opercular and insular region: a pilot study. **Acta Neurochir 132:**66–74, 1995
6. Hentschel SJ, Lang FF: Surgical resection of intrinsic insular tumors. **Neurosurgery 57 (1 Suppl):**176–183, 2005
7. Higano S, Yun X, Kumabe T, Watanabe M, Mugikura S, Umetsu A, et al: Malignant astrocytic tumors: clinical importance of apparent diffusion coefficient in prediction of grade and prognosis. **Radiology 241:**839–846, 2006
8. Kitis O, Altay H, Calli C, Yunten N, Akalin T, Yurtseven T: Minimum apparent diffusion coefficients in the evaluation of brain tumors. **Eur J Radiol 55:**393–400, 2005
9. Kumabe T, Nakasato N, Suzuki K, Sato K, Sonoda Y, Kawagishi J, et al: Two-staged resection of a left frontal astrocytoma involving the operculum and insula using intraoperative neurophysiological monitoring—case report. **Neurol Med Chir 38:**503–507, 1998
10. Lang FF, Olansen NE, DeMonte F, Gokaslan ZL, Holland EC, Kalhorn C, et al: Surgical resection of intrinsic insular tumors: complication avoidance. **J Neurosurg 95:**638–650, 2001
11. LeRoux PD, Berger MS, Haglund MM, Pilcher WH, Ojemann GA: Resection of intrinsic tumors from nondominant face motor cortex using stimulation mapping: report of two cases. **Surg Neurol 36:**44–48, 1991
12. Peraud A, Ilmberger J, Reulen HJ: Surgical resection of gliomas WHO grade II and III located in the opercular region. **Acta Neurochir 146:**9–18, 2004
13. Phan TG, Donnan GA, Wright PM, Reutens DC: A digital map of middle cerebral artery infarcts associated with middle cerebral artery trunk and branch occlusion. **Stroke 36:**986–991, 2005
14. Schaefer PW, Grant PE, Gonzalez RG: Diffusion-weighted MR imaging of the brain. **Radiology 217:**331–345, 2000
15. Smith JS, Cha S, Mayo MC, McDermott MW, Parsa AT, Chang SM, et al: Serial diffusion-weighted magnetic resonance imaging in cases of glioma: distinguishing tumor recurrence from postresection injury. **J Neurosurg 103:**428–438, 2005
16. Sugahara T, Korogi Y, Kochi M, Ikushima I, Shigematu Y, Hirai T, et al: Usefulness of diffusion-weighted MRI with echo-planar technique in the evaluation of cellularity in gliomas. **J Magn Reson Imaging 9:**53–60, 1999
17. Takahashi S, Goto K, Fukasawa H, Kawata Y, Uemura K, Suzuki K: Computed tomography of cerebral infarction along the distribution of the basal perforating arteries. Part I: Striate arterial group. **Radiology 155:**107–118, 1985
18. Takahashi S, Goto K, Fukasawa H, Kawata Y, Uemura K, Yaguchi K: Computed tomography of cerebral infarction along the distribution of the basal perforating arteries. Part II: Thalamic arterial group. **Radiology 155:**119–130, 1985
19. Tanriover N, Rhoton AL Jr, Kawashima M, Ulm AJ, Yasuda A: Microsurgical anatomy of the insula and the sylvian fissure. **J Neurosurg 100:**891–922, 2004
20. Ture U, Yaşargil MG, Al-Mefty O, Yaşargil DC: Arteries of the insula. **J Neurosurg 92:**676–687, 2000
21. Zimmerman RD: Is there a role for diffusion-weighted imaging in patients with brain tumors or is the "bloom off the rose"? **AJNR 22:**1013–1014, 2001

Manuscript submitted March 26, 2006.
Accepted August 7, 2006.

Address reprint requests to: Toshihiro Kumabe, M.D., Department of Neurosurgery, Tohoku University Graduate School of Medicine, 1–1 Seiryo-machi, Aoba-ku, Sendai 980–8574, Japan. email: kuma@nsg.med.tohoku.ac.jp.

J Neurooncol
DOI 10.1007/s11060-006-9247-5

LABORATORY INVESTIGATION

Safety and efficacy of convection-enhanced delivery of ACNU, a hydrophilic nitrosourea, in intracranial brain tumor models

Shin-ichiro Sugiyama · Yoji Yamashita · Toshio Kikuchi · Ryuta Saito · Toshihiro Kumabe · Teiji Tominaga

Received: 21 June 2006 / Accepted: 11 August 2006

Abstract Convection-enhanced delivery (CED) is a local infusion technique, which delivers chemotherapeutic agents directly to the central nervous system, circumventing the blood–brain barrier and reducing systemic side effects. CED distribution is significantly increased if the infusate is hydrophilic. This study evaluated the safety and efficacy of CED of nimustine hydrochloride: 3-[(4-amino-2-methyl-5-pyrimidinyl) methyl]-1-(2-chloroethyl)-1-nitrosourea hydrochloride (ACNU), a hydrophilic nitrosourea, in rat 9 L brain tumor models. The local neurotoxicity of ACNU delivered via CED was examined in normal rat brains, and the maximum tolerated dose (MTD) was estimated at 0.02 mg/rat. CED of ACNU at the MTD produced significantly longer survival time than systemic administration ($P < 0.05$, log-rank test). Long-term survival (80 days) and eradication of the tumor occurred only in the CED-treated rats. The tissue concentration of ACNU was measured by high-performance liquid chromatography, which revealed that CED of ACNU at the dose of 100-fold less total drug than intravenous injection carried almost equivalent concentrations of ACNU into rat brain tissue. CED of hydrophilic ACNU is a promising strategy for treating brain tumors.

Keywords Brain tumor · Convection-enhanced delivery · High-performance liquid chromatography · Nimustine hydrochloride · Nitrosourea

S. Sugiyama · Y. Yamashita (✉) ·
T. Kikuchi · R. Saito · T. Kumabe · T. Tominaga
Department of Neurosurgery, Tohoku University Graduate School of Medicine, 1-1 Seiryo-machi, Aoba-ku, Sendai 980-8574, Japan
e-mail: yoji@nsg.med.tohoku.ac.jp

Abbreviations

ACNU	3-[(4-amino-2-methyl-5-pyrimidinyl) methyl]-1-(2-chloroethyl)-1-nitrosourea hydrochloride
BBB	Blood-brain barrier
BCNU	1,3-bis-chlorethyl-1-nitrosourea
CED	Convection-enhanced delivery
CNS	Central nervous system
HBSS	Hanks balanced salt solution
H&E	Hematoxylin and eosin
i.v.	Intravenous
MTD	Maximum tolerated dose

Introduction

Prognosis for the patients with high-grade gliomas remains dismal. Recently, Stupp et al. [1] demonstrated that radiotherapy plus concomitant and adjuvant temozolomide, a novel oral alkylating agent, is well tolerated and improves survival in patients with newly diagnosed glioblastoma. However, the activity of temozolomide is still not satisfactory in malignant gliomas. Poor penetration of most anti-cancer drugs across the blood–brain barrier (BBB) into the central nervous system (CNS) remains a major obstacle in the application of systemic chemotherapy for intracranial malignancies [2, 3]. Even using agents that penetrate the BBB, tumoricidal drug concentrations are difficult to reach brain tumor tissue without incurring unacceptable systemic side effects.

Convection-enhanced delivery (CED) was introduced in 1994 as a strategy to overcome such difficulties

[4]. Utilizing bulk flow, CED allows the direct delivery of small or large molecules to a targeted site, offering an improved volume of distribution compared to simple diffusion. CED bypasses the BBB, delivers a high concentration of therapeutic agents to the injection site, provides wider distribution of therapeutic agents within the target site, and minimizes systemic exposure, resulting in fewer systemic side effects. In addition, CED provides homogeneous distribution of infusate, which drop off sharply at the edge in normal brain tissue, resulting in delivery of the therapeutic agent to the entire targeted region while limiting the potential for widespread neurotoxicity [5].

Nitrosoureas have been important in systemic chemotherapy for high-grade gliomas for decades. 1,3-bischlorethyl-1-nitrosourea (BCNU) had the most proven efficacy, but the effects on clinical outcome have been limited [6]. Dose escalation of BCNU to increase the efficacy against gliomas has been hampered by severe systemic toxicity to the bone marrow, lungs, and kidneys [7]. To avoid such systemic toxicities, local delivery methods, including direct injection and biodegradable polymers or wafers, have been used, but only offered modest improvements to the overall survival rates for patients with malignant gliomas [8–13]. Those delivery methods yielded limited diffusion and distribution of drug into the surrounding tissues, which is typically not more than a few millimeters [13].

Convection-enhanced delivery has the potential to deliver an efficient volume of BCNU to targeted sites without systemic exposure. BCNU could be safely and effectively administered via CED in the rat glioma model to shrink gliomas with little or no toxicity [14]. However, BCNU is not the ideal drug for CED because the log p of BCNU is 1.53, which means that BCNU is lipophilic [15] (log p is the log of the octanol/water partition coefficient [16]). For CED injection, it needs to dissolve in organic solvent like ethanol that has nonspecific cytotoxity in itself. Furthermore, the water solubility of drugs limits the volume of distribution within the brain tissue and CED distributed lipophilic drugs less widely than hydrophilic agents [11, 12].

3-[(4-amino-2-methyl-5-pyrimidinyl) methyl]-1-(2-chloroethyl)-1-nitorosourea hydrochloride (ACNU), is the first water-soluble nitrosourea compound discovered in 1974 [17]. ACNU dissolves in water easily as a cationic ion. The log p of ACNU is 0.92 [17], which means that ACNU is lipophilic as well as hydrophilic, because ACNU changes from cationic ion to neutral compound under physiological conditions. In clinical protocols against high-grade gliomas, systemic administration of ACNU has proven efficacy but also dose-limiting myelotoxicity like BCNU [18, 19].

We hypothesized that CED of ACNU would be therapeutically advantageous over systemic administration for treating intracranial malignancies, because CED could distribute hydrophilic ACNU over the entire targeted region and deliver a high concentration of ACNU without systemic exposure. This study examined the safety and efficacy of CED with ACNU in rat 9 L brain tumor models.

Materials and methods

ACNU

ACNU was provided by Sankyo Co. Ltd. (Tokyo, Japan). Infusion solutions of ACNU were prepared by diluting ACNU in saline to a concentration of 10, 5, 2, 1, 0.5, 0.2, and 0.1 mg/mL.

Tumor cell line

The 9 L gliosarcoma cells (American Type Culture Collection, Rockville, MD, USA) were maintained as monolayers in a complete medium consisting of Eagle's minimal essential medium supplemented with 10% fetal calf serum, non-essential amino acids, and 100 U/mL penicillin G. Cells were cultured at 37°C in a humidified atmosphere consisting of 95% air and 5% CO_2.

Animals and intracranial xenograft technique

All protocols used in the animal studies were approved by the Institute for Animal Experimentation of Tohoku University Graduate School of Medicine.

Male Fisher 344 rats weighing approximately 200 g were purchased from Charles-River Laboratories (Charles-River Japan Inc., Tsukuba, Japan). For the intracranial xenograft tumor model, 9 L gliosarcoma cells were harvested by trypsinization, washed once with Hanks balanced salt solution without Ca^{++} and Mg^{++} (HBSS), and resuspended in HBSS for implantation. Cells (5×10^5) in 10 μL HBSS were implanted into the striatal region of Fisher 344 rat brains as follows: under deep isoflurane anesthesia, rats were placed in a small-animal stereotactic frame (David Kopf Instrument, Tujunga, CA, USA). A sagittal incision was made to expose the cranium followed by a burr hole in the skull at 0.5 mm anterior and 3 mm lateral from the bregma using a small dental drill. Cell suspension (5 μL) was injected over 2 min at a depth of 4.5 mm from the brain surface; after a 2-minute wait, another 5 μL were injected over 2 min at a depth of

4.0 mm, and after a final 2-minute wait, the needle was removed and the wound was sutured.

CED

Convection-enhanced delivery of ACNU or saline was done using a volume of 20 μL as described previously [20]. Briefly, the infusion system consisted of a reflux-free step-design infusion cannula (as described [21]) connected to a loading line (containing ACNU or saline) and an olive oil infusion line. A 1-mL syringe (filled with oil) mounted onto a micro-infusion pump (BeeHive; Bioanalytical Systems, West Lafayette, IN, USA) regulated the flow of fluid through the system. Based on chosen coordinates, the infusion cannula was mounted onto stereotactic holders and guided to the target region of the brain through burr holes made in the skull. The following ascending infusion rates were applied to achieve the 20-μL total infusion volume: 0.2 μL/min (15 min) + 0.5 μL/min (10 min) + 0.8 μL/min (15 min).

Evaluation of toxicity

Healthy male Sprague–Dawley rats weighing approximately 200 g (Charles-River Japan Inc.) received a single 20-μL CED infusion of ACNU at doses of 0.2, 0.1, 0.04, 0.02, 0.01, 0.004, or 0.002 mg/rat (six per group). Rats were monitored daily for survival, weekly weights, and general health (alertness, grooming, feeding, excreta, skin, fur, mucous membrane conditions, ambulation, breathing, and posture). Three rats in each group were euthanized on the 30th or the 60th day after the CED treatment, and their brains were removed, fixed, subjected to paraffin sectioning (5 μm), and stained with hematoxylin and eosin (H&E).

Survival studies

Forty rats with 9 L tumor cells were randomly assigned to five groups: (a) the control group, receiving CED of saline ($n = 8$); (b) the systemic treatment group, receiving intravenous (i.v.) injection of ACNU at a dose of 0.4 mg/rat (2 mg/kg: clinically tolerable dose for i.v. administration [17]) ($n = 8$); and (c)–(e) CED groups, receiving CED of ACNU at a dose of 0.005 mg/rat ($n = 8$), 0.01 mg/rat ($n = 8$), and 0.02 mg/rat ($n = 8$). Seven days after tumor cell implantation, a single CED infusion (20 μL; 1 mg/mL or 0.5 mg/mL ACNU) or a bolus i.v. injection via a tail vein (0.4 mL; 0.1 mg/mL ACNU) was performed for each group. Rats were monitored daily for survival and general health. Animal weights were reported weekly. The study was terminated 80 days after tumor implantation, when the surviving animals were euthanized and their brains stained with H&E.

Results for the survival studies are expressed as a Kaplan–Meier curve. Survival between the treatment groups was compared with a log-rank test.

High-performance liquid chromatography for ACNU in rat brain tissue

Normal Sprague–Dawley rats weighing approximately 200 g (Charles-River Japan Inc.) were given a single 20-μL infusion by CED of ACNU at 0.02 mg/rat or a bolus i.v. injection of ACNU at 2.0 mg/rat or 0.4 mg/rat (nine rats per group). Three rats were sacrificed at 0, 2, or 4 h after the treatments. The appropriate brain hemisphere was perfused with phosphate buffered saline, surgically removed, and frozen. All samples were stored at -80°C to avoid deterioration until biochemical measurements were carried out (within a month of brain dissection). Phosphoric acid buffer (0.1 mol/L) was added to the tissues at an 80% ratio (v/w), and the tissue was homogenized using a mechanical homogenizer. Fluoranthene (0.8 μg, internal standard) and *n*-hexane (5 mL) was added to the homogenates (0.5 mL). The mixture was shaken for 5 min and centrifuged at 3,000 rpm for 5 min, then the *n*-hexane layer was extracted and evaporated. The remnant was dissolved in 6% acetonitrile (200 μL) and injected into the chromatographic column (4.6 × 150 mm^2; Nova-Pack C18; Waters, Milford, MA, USA). Analysis was conducted on LC-10A system (Shimadzu Co., Kyoto, Japan). The mobile phase consisted of 6% acetonitrile, refined water, and 1 g/L sodium heptanesulphonate (PIC B7) (77 : 23 : 0.4). All separations were performed isocratically at a flow rate of 1.0 mL/min at room temperature. ACNU was typically eluted in 3 min, and detected by ultraviolet at 254 nm.

Results

Toxicity of ACNU in normal rodent CNS

Dose-limiting local toxicity occurred at 0.04 mg/rat or over, establishing the maximum tolerated dose (MTD) at 0.02 mg/rat (Fig. 1). All animals that received CED of ACNU at 0.04 mg/rat or over had extensive tissue necrosis within the CNS (Fig. 1a). Animals receiving CED of ACNU at 0.02 mg/rat or under showed evidence of minor trauma at the site of the infusion cannula in the striatum but otherwise no apparent tissue toxicity (Fig. 1b, c).

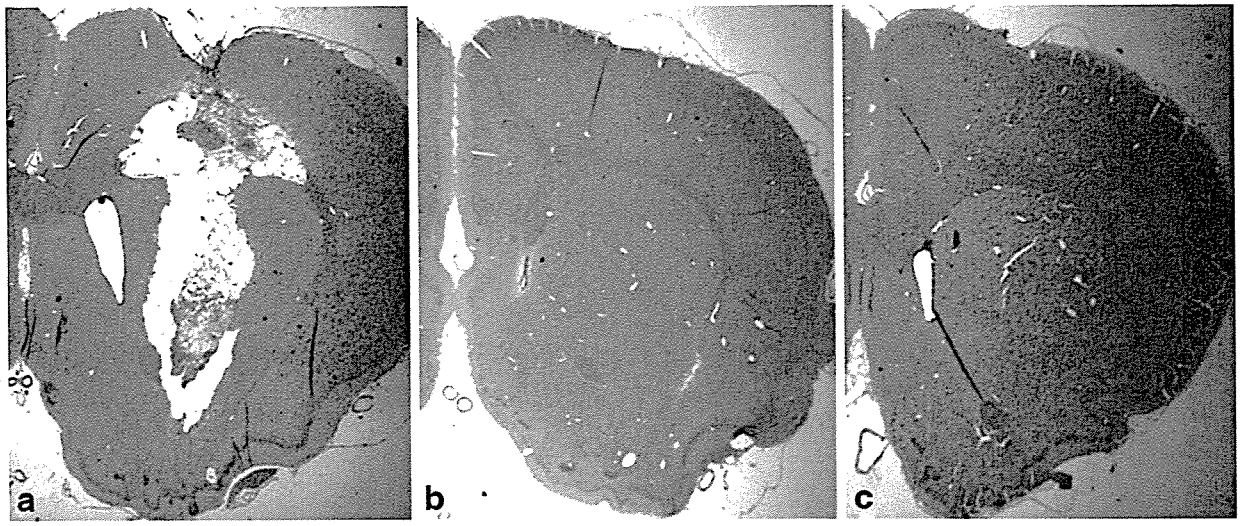

Fig. 1 Local tissue toxicity of ACNU administered via CED in the normal adult rat brain. Rat brains were treated with a single CED infusion of ACNU at different seven doses (0.2, 0.1, 0.04, 0.02, 0.01, 0.004, or 0.002 mg/rat). Representative H&E sections from three groups on the 30th day after CED. Extensive tissue injury was observed in animals treated with more than 0.04 mg/rat (**a**: 0.1 mg/rat). Rats treated with less than 0.02 mg showed no drug-induced damages (**b**: 0.02 mg/rat, **c**: 0.01 mg/rat)

No systemic toxicities were observed following CED of ACNU even at or over MTD. Furthermore, even the extensive CNS damage caused by ACNU resulted in no neurological symptoms.

Anti-tumor efficacy of ACNU through CED or intravenous administration

The anti-tumor efficacy of ACNU delivered via CED at the tested MTD (0.02 mg/rat) and half MTD (0.01 mg/rat) was compared with that of ACNU administered systemically at 0.4 mg/rat in the intracranial 9 L tumor model. The control group received CED infusion of saline.

As shown in Fig. 2, all animals in the control group expired due to tumor progression by day 21 and mean survival was only 16.5 days (median, 16.5 days). Systemic treatment with ACNU showed no improvement in survival. All animals expired by day 33 and mean survival was 19 days (median, 17 days). Animals treated with CED of ACNU at the dose of 0.005 mg/rat also expired by day 29 and mean survival was 18.2 days (median, 16.5 days). There was no significant advantage compared with the control group. Animals treated with CED of ACNU at the dose of 0.01 mg/rat expired by day 49 and mean survival was 26.5 days (median, 19.5 days). Although this CED treatment group showed a slight improvement in survival, there was no significant advantage compared with the group receiving i.v. administration of ACNU. Animals treated with CED of ACNU at the MTD of 0.02 mg/rat showed significantly improved survival rate compared with i.v. administration of ACNU ($p < 0.05$, log-rank test); treatment at the 0.02 mg/rat resulted in two of eight animals (25%) surviving beyond day 80 (median, 26.5 days).

Histopathologic evaluation of brain tissue was done in all animals at death or after sacrifice. Animals showing clinical signs of tumor progression were euthanized. Two animals survived to the study end at day 80, in the group receiving CED infusion of ACNU at the MTD (0.02 mg/rat), and showed complete pathologic responses (Fig. 3a). Tumor progression was observed in the brains of all rats, which died (Fig. 3b).

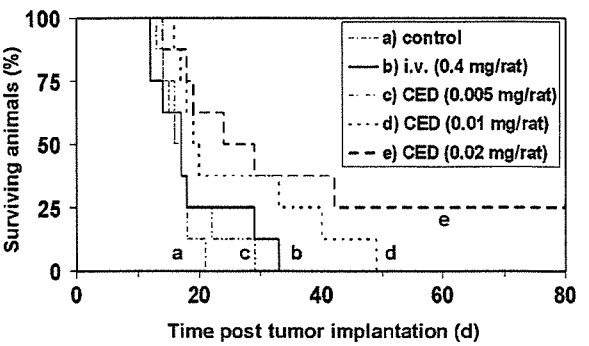

Fig. 2 Treatment of rats bearing 9 L tumors with CED or i.v. administration of ACNU. Seven days after tumor implantation within the brain, rats were treated with CED of saline (**a**), i.v. administration of ACNU at 0.4 mg/rat (**b**), and CED of ACNU at 0.005 mg/rat (**c**), 0.01 mg/rat (**d**), and 0.02 mg/rat (**e**). Eight animals per group

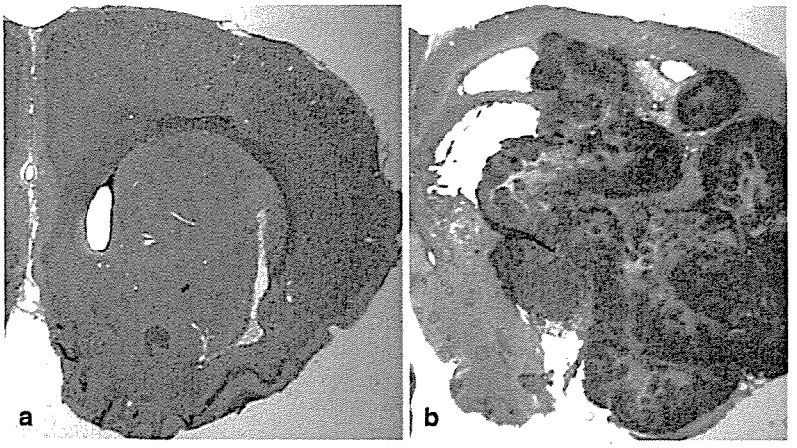

Fig. 3 Representative brain sections from surviving and non-surviving animals. (**a**) Brain section obtained from one of the survivors treated by CED of ACNU at 0.02 mg/rat. Neither survivor had residual tumor. (**b**) Brain section from a rat of the control group showing a typical tumor found in all non-surviving animals in which tumor progression led to death

Tissue concentration of ACNU following CED or intravenous administration

The mean tissue concentrations just after the treatment with CED of ACNU at the dose of 0.02 mg/rat, and i.v. injection of ACNU at 2.0 and 0.4 mg/rat were 3.21, 3.47, and 0.52 μg/g, respectively. CED of ACNU at the dose of 100-fold less total drug than i.v. injection carried an almost equivalent concentration of ACNU into rat brain tissue. The tissue concentration after treatment with CED at the dose of 0.02 mg/rat was almost as high as that of i.v. administration at the dose of 2.0 mg/rat, and was about six times as high as that of i.v. administration at the dose of 0.4 mg/rat. ACNU was completely cleared from the brain tissues within 4 h in all groups (Fig. 4).

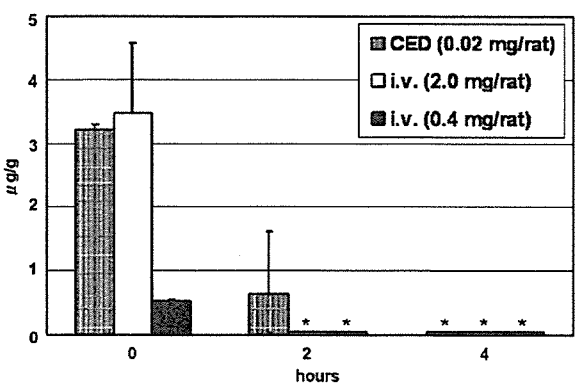

Fig. 4 Tissue concentrations of ACNU in the normal rat brain following single CED infusion and bolus i.v. injection. Drug concentrations were measured by high-performance liquid chromatography assay for ACNU. *: below the detection limit of 0.05 μ g/g

Discussion

Convection-enhanced delivery has shown considerable potential for the treatment of brain tumors, with some of the protocols now in clinical trials [5, 22]. ACNU is a hydrophilic nitrosourea with a proven efficacy against high-grade gliomas through systemic administration [18, 19]. Our studies demonstrated that combining ACNU with the CED technique provided safe and significant anti-tumor effects in animal brain tumor models.

To evaluate the safe dose of ACNU via CED, we performed the toxicity test in the normal brain parenchyma of intact rats. The established MTD was 0.02 mg/rat (1.0 mg/mL ACNU, 20 μL CED). This dose was far smaller than the clinically tolerable dose of 0.4 mg/rat for systemic administration, and CED at the dose of 0.02 mg/rat resulted in no systemic complication.

3-[(4-amino-2-methyl-5-pyrimidinyl) methyl]-1-(2-chloroethyl)-1-nitrosourea hydrochloride is lipophilic as well as hydrophilic under physiological conditions ($\log p = 0.92$). Hydrophilic ACNU delivered via CED is expected to distribute over the extracellular space of the brain, gradually becoming lipophilic, then taken up into the surrounding cells, and manifesting the anti-cancer effect.

As confirmed by high-performance liquid chromatography, ACNU administered via CED yielded much higher drug levels in brain tissue than i.v. administration. The survival study using 9 L rat brain tumor models revealed that CED infusion at the MTD of ACNU produced significantly improved survival rate compared with i.v. administration, and the anti-tumor effect of ACNU delivered via CED was dose-dependent. These results demonstrated that CED enhanced

the anti-tumor effect of hydrophilic ACNU compared with i.v. administration.

Infusion of a high concentration of ACNU resulted in increased local CNS toxicity, which was ascribed to the non-specific cytotoxicity of ACNU. The local neurotoxicity strictly limited the therapeutic window of ACNU delivered via CED, so we could not attempt dose escalation to increase the anti-tumor effect of ACNU. Several studies have utilized drug encapsulation in nano-particles to overcome such non-specific cytotoxicity of anticancer drugs [23–25]. Encapsulation of drugs increases tissue tolerance by reducing the acute tissue exposure and slowing the rate of drug release. Encapsulated ACNU in nano-particles may allow a higher dose of ACNU to be delivered via CED.

The short-tissue retention time of ACNU was another limiting factor of the anti-tumor efficacy in our study. ACNU infused via CED was completely cleared from the brain tissue within 4 h. Unencapsulated and water-soluble agents are typically cleared from the brain in less than one day [23, 24]. Furthermore, if the molecular weight of the agent is < 200–400, free exchange takes place between plasma and brain extracellular water across the BBB [15]. The rapid clearance of ACNU may be partially due to its small molecular weight (309.15). To extend the drug residence, encapsulation of drugs in nano-particles as described above is also possible. Encapsulated agents have prolonged tissue residence time in CED compared with free agents [23, 24]. Combining drug encapsulation techniques with CED may reduce CNS toxicity as well as increase tissue retention and anti-tumor efficacy.

The survival rate of animals treated with CED of ACNU at the dose of 0.02 mg/rat (0.1 mg/kg) was 25%. Presumably the difference between survivors and non-survivors within the same CED group could be attributed to the inhomogeneous drug distribution within the tumors. Heterogeneous distribution of anti-cancer drugs results in partial response and local recurrence of brain neoplasms [5, 26]. Current ongoing clinical CED lacks monitoring or confirmation of the drug distribution [5, 22], although several infusion sites can be selected to optimize catheter placement and achieve homogeneous drug distribution over the entire targeted lesion [5]. Further animal studies with CED are needed to improve the drug distribution in human brain tumors.

Several studies support the applicability of ACNU administered via CED to clinical treatment of high-grade gliomas in humans. Locally injected ACNU into recurrent gliomas was effective in inducing tumor necrosis and inhibiting tumor growth [27]. Intraventricular administration of ACNU is safe and efficacious in the treatment of malignant gliomas [28–30]. The present study also suggests that CED of ACNU is capable of increasing efficacy in the field of glioma treatment.

References

1. Stupp R, Mason WP, van den Bent MJ, Weller M, Fisher B, Taphoorn MJ, Belanger K, Brandes AA, Marosi C, Bogdahn U, Curschmann J, Janzer RC, Ludwin SK, Gorlia T, Allgeier A, Lacombe D, Cairncross JG, Eisenhauer E, Mirimanoff RO, European Organisation for Research, Treatment of Cancer Brain Tumor and Radiotherapy Groups, National Cancer Institute of Canada Clinical Trials Group (2005) Radiotherapy plus concomitant and adjuvant temozolomide for glioblastoma. N Engl J Med 352(10):987–996
2. Stewart LA (2002) Chemotherapy in adult high-grade glioma: a systematic review and meta-analysis of individual patient data from 12 randomised trials. Lancet 359:1011–1018
3. Groothuis DR (2000) The blood-brain and blood-tumor barriers: a review of strategies for increasing drug delivery. Neuro-oncol 2:45–59
4. Bobo RH, Laske DW, Akbasak A, Morrison PF, Dedrick RL, Oldfield EH (1994) Convection-enhanced delivery of macromolecules in the brain. Proc Natl Acad Sci USA 91:2076–2080
5. Vogelbaum MA (2005) Convection enhanced delivery for the treatment of malignant gliomas: symposium review. J Neurooncol 73:57–69
6. Mahaley MS Jr (1991) Neuro-oncology index and review (adult primary brain tumors). Radiotherapy, chemotherapy, immunotherapy, photodynamic therapy. J Neurooncol 11:85–147
7. Gilmann AG, Goodman LS, Rall TW, Murad TW (eds) (1985) Goodman and Gilman's the pharmacological basis of therapeutics, 7th edn. Macmillan, New York, pp 1260–1261
8. Walter KA, Tamargo RJ, Olivi A, Burger PC, Brem H (1995) Intratumoral chemotherapy. Neurosurgery 37:1128–1145
9. Brem H, Piantadosi S, Burger PC, Walker M, Selker R, Vick NA, Black K, Sisti M, Brem S, Mohr G, Muller P, Morawetz R, Schold SC (1995) Placebo-controlled trial of safety and efficacy of intraoperative controlled delivery by biodegradable polymers of chemotherapy for recurrent gliomas. Lancet 345:1008–1012
10. Westphal M, Hilt DC, Bortey E, Delavault P, Olivares R, Warnke PC, Whittle IR, Jaaskelainen J, Ram Z (2003) A phase 3 trial of local chemotherapy with biodegradable carmustine (BCNU) wafers (Gliadel wafers) in patients with primary malignant glioma. Neuro-oncol 5:79–88
11. Saito R, Krauze MT, Noble CO, Tamas M, Drummond DC, Kirpotin DB, Berger MS, Park JW, Bankiewicz KS (2006) Tissue affinity of the infusate affects the distribution volume during convection-enhanced delivery into rodent brains: Implications for local drug delivery. J Neurosci Methods 9:S0165–S0270
12. Buahin KG, Brem H (1995) Interstitial chemotherapy of experimental brain tumors: comparison of intratumoral injection versus polymeric controlled release. J Neurooncol 26:103–110
13. Fleming AB, Saltzman WM (2002) Pharmacokinetics of the carmustine implant. Clin Pharmacokinet 41:403–419
14. Bruce JN, Falavigna A, Johnson JP, Hall JS, Birch BD, Yoon JT, Wu EX, Fine RL, Parsa AT (2000) Intracerebral clysis in a rat glioma model. Neurosurgery 46:683–691

15. Walker MD, Hilton J (1976) Nitrosourea pharmacodynamics in relation to the central nervous system. Cancer Treat Rep 60:725–728
16. Hansch C, Smith N, Engle R, Wood H (1972) Quantitative structure-activity relationships of antineoplastic drugs: nitrosoureas and triazenoimidazoles. Cancer Chemother Rep 56:443–456
17. Mori T, Mineura K, Katakura R (1979) Chemotherapy of malignant brain tumor by a water-soluble anti-tumor nitrosourea, ACNU. Neurol Med Chir (Tokyo) 19:1157–1171
18. Takakura K, Abe H, Tanaka R, Kitamura K, Miwa T, Takeuchi K, Yamamoto S, Kageyama N, Handa H, Mogami H et al (1986) Effects of ACNU and radiotherapy on malignant glioma. J Neurosurg 64:53–57
19. Weller M, Muller B, Koch R, Bamberg M, Krauseneck P, Neuro-Oncology Working Group of the German Cancer Society (2003) Neuro-oncology Working Group 01 trial of nimustine plus teniposide versus nimustine plus cytarabine chemotherapy in addition to involved-field radiotherapy in the first-line treatment of malignant glioma. J Clin Oncol 21:3276–3284
20. Saito R, Bringas JR, McKnight TR, Wendland MF, Mamot C, Drummond DC, Kirpotin DB, Park JW, Berger MS, Bankiewicz KS (2004) Distribution of liposomes into brain and rat brain tumor models by convection-enhanced delivery monitored with magnetic resonance imaging. Cancer Res 64:2572–2579
21. Krauze MT, Saito R, Noble C, Tamas M, Bringas J, Park JW, Berger MS, Bankiewicz K (2005) Reflux-free cannula for convection-enhanced high-speed delivery of therapeutic agents. J Neurosurg 103:923–929
22. Kunwar S (2003) Convection enhanced delivery of IL13-PE38QQR for treatment of recurrent malignant glioma: presentation of interim findings from ongoing phase 1 studies. Acta Neurochir Suppl 88:105–111
23. Noble CO, Krauze MT, Drummond DC, Yamashita Y, Saito R, Berger MS, Kirpotin DB, Bankiewicz KS, Park JW (2006) Novel nanoliposomal CPT-11 infused by convection-enhanced delivery in intracranial tumors: pharmacology and efficacy. Cancer Res 66:2801–2806
24. Saito R, Krauze MT, Noble CO, Drummond DC, Kirpotin DB, Berger MS, Park JW, Bankiewicz KS (2006) Convection-enhanced delivery of Ls-TPT enables an effective, continuous, low-dose chemotherapy against malignant glioma xenograft model. Neuro-oncol 24:S1522–S8517
25. Yamashita Y, Saito R, Krauze MT, Kawaguchi T, Noble CO, Drummond DC, Kirpotin DB, Berger MS, Park JW, Berger MS, Bankiewicz KS (2006) Convection-enhanced delivery of liposomal doxorubicin in intracranial brain tumor xenografts. Targeted Oncol 1:79–85
26. Vavra M, Ali MJ, Kang EW, Navalitloha Y, Ebert A, Allen CV, Groothuis DR (2004) Comparative pharmacokinetics of 14C-sucrose in RG-2 rat gliomas after intravenous and convection-enhanced delivery. Neuro-oncol 6:104–112
27. Wakabayashi T, Yoshida J, Mizuno M, Kajita Y (2001) Intratumoral microinfusion of nimustine (ACNU) for recurrent glioma. Brain Tumor Pathol 18:23–28
28. Levin VA, Byrd D, Campbell J, Giannini DD, Borcich JK, Davis RL (1985) Central nervous system toxicity and cerebrospinal fluid pharmacokinetics of intraventricular 3-[(4-amino-2-methyl-5-pyrimidinyl)ethyl]-1-(2-chloroethyl)-1-nitro soureas and other nitrosoureas in beagles. Cancer Res 45:3803–3809
29. Ushio Y, Kochi M, Kitamura I, Kuratsu J (1998) Ventriculolumber perfusion of 3-[(4-amino-2-methyl-5-pyrimidinyl)-methyl]-1-(2-chloroethyl-1-nitrosourea hydrochloride for subarachnoid dissemination of gliomas. J Neurooncol 38:207–212
30. Kochi M, Kuratsu J, Mihara Y, Takaki S, Seto H, Uemura S, Ushio Y (1993) Ventriculolumbar perfusion of 3-[(4-amino-2-methyl-5-pyrimidinyl)methyl]-1-(2-chloroethyl)-1-nitrosourea hydrochloride. Neurosurgery 33:817–823

Malignant Astrocytic Tumors: Clinical Importance of Apparent Diffusion Coefficient in Prediction of Grade and Prognosis[1]

Shuichi Higano, MD, PhD
Xia Yun, MD, PhD
Toshihiro Kumabe, MD, PhD
Mika Watanabe, MD, PhD
Shunji Mugikura, MD, PhD
Atsushi Umetsu, MD, PhD
Akihiro Sato, MD, PhD
Takayuki Yamada, MD, PhD
Shoki Takahashi, MD, PhD

Purpose: To retrospectively assess the apparent diffusion coefficient (ADC) for prediction of malignancy and prognosis of malignant astrocytic tumors.

Materials and Methods: The institutional review board approved this study and did not require patient informed consent. Findings from 37 consecutive patients (21 men, 16 women; mean age, 43 years) with pathologically proved malignant astrocytic tumors that included 22 glioblastomas (GBMs) and 15 anaplastic astrocytomas (AAs) were retrospectively evaluated. The minimum ADC value of each tumor was preoperatively determined from several regions of interest defined in the tumor, preferably with avoidance of cystic or necrotic components, on ADC maps derived from isotropic diffusion-weighted images. Surgical intervention, followed by radiation therapy, was undertaken in all cases according to hospital protocol. Immunohistologically, Ki-67 labeling index (LI), indicating cell proliferation, was also determined. The patients were classified into two groups, progressive and stable, according to the 2-year observation after the initial treatment. Correlation analysis (Pearson product moment correlation), Student *t* test, Welch test, receiver operating characteristic analysis, and Kaplan-Meier method with log-rank test were used for statistical evaluation.

Results: There was a significant negative correlation between minimum ADC and Ki-67 LI ($r = -0.562$, $P < .001$). The mean minimum ADC (0.834×10^{-3} mm$^2 \cdot$ sec^{-1}) of GBM was significantly lower than that (1.06×10^{-3} mm$^2 \cdot$ sec^{-1}) of AA ($P < .001$, Student *t* test). The mean minimum ADC (0.80×10^{-3} mm$^2 \cdot$ sec^{-1}) of the progressive group was significantly lower than that (1.037×10^{-3} mm$^2 \cdot$ sec^{-1}) of the stable group ($P < .001$). The cutoff value of 0.90×10^{-3} mm$^2 \cdot$ sec^{-1} for minimum ADC for differentiation of patients with a favorable prognosis from those with a poor prognosis provided the best combination of sensitivity (79%) and specificity (81%) (receiver operating characteristic analysis). The significant difference in the prognosis between two groups classified by using this cutoff value of minimum ADC was noted ($P = .002$, log-rank test).

Conclusion: The minimum ADC of malignant astrocytomas can provide additional information about their clinical malignancy related to posttreatment prognosis.

[1] From the Departments of Diagnostic Radiology (S.H., S.M., A.U., A.S., T.Y., S.T.), Neuroendovascular Therapy (X.Y.), and Neurosurgery (T.K.), Tohoku University Graduate School of Medicine, 1-1 Seiryo-machi Aoba-ku, Sendai, Miyagi, 980-8574, Japan; and Department of Pathology, Tohoku University Hospital, Tohoku, Japan (M.W.). Received July 31, 2005; revision requested October 7; revision received November 15; accepted December 8; final version accepted February 3, 2006. **Address correspondence to** S.H. (e-mail: *higano-s@rad.med.tohoku.ac.jp*).

Astrocytic tumors are the most common primary brain neoplasms and account for more than 70% of all gliomas (1). The overall prognosis of malignant astrocytic tumors, especially glioblastomas (GBMs), is still poor in spite of aggressive treatments (1,2). In the clinical setting, however, the prognosis of these tumors varies from patient to patient; some patients have a relatively favorable prognosis, and others have a very poor prognosis, despite the same histopathologic diagnosis and equivalent treatments.

More exact pathologic evaluation of tumor malignancy that might closely correlate with the patient's prognosis would affect treatment planning. Ki-67 labeling index (LI) is one such optional immunohistochemical examination for the evaluation of tumor proliferation (3–6). This index has become an important part of histologic assessments and postsurgical assignment of grade for brain tumors, as a higher rate of Ki-67–positive cells corresponds to a greater malignancy of brain tumors. This method, however, is applicable to tumor specimens obtained at surgical intervention. The method that enables preoperative assessment of tumor malignancy to make a more effective therapeutic strategy possible for improvement in the prognosis has long been awaited.

Introduction of diffusion-weighted (DW) magnetic resonance (MR) imaging has enabled us to obtain additional information derived from microscopic motion of the water proton, which is not available by using conventional MR imaging. DW imaging has been applied for assignment of tumor grades or differentiation of tumors, as well as for diagnosis of ischemic stroke (7–14). Several investigators found an inverse correlation between the apparent diffusion coefficient (ADC) calculated from DW images and tumor cellularity (7,8,11,14,15). Some studies involving the assignment of grades to gliomas by using ADC showed the usefulness of ADC for such assignment (9,14), but others did not (12). To our knowledge, there has been no report in which preoperative assessment of ADC for prediction of posttherapeutic prognosis was discussed. Thus, the purpose of our study was to retrospectively assess the use of the ADC for the prediction of malignancy and the prognosis of malignant astrocytic tumors.

Advances in Knowledge

- The minimum apparent diffusion coefficient (ADC) values of malignant astrocytic tumors are negatively correlated with the Ki-67 labeling index.
- A significant difference ($P < .001$) in minimum ADC values was noted between anaplastic astrocytoma and glioblastoma.
- The mean minimum ADC value of patients with a favorable prognosis was significantly higher ($P < .001$) than it was for those with a poor prognosis.
- By using a threshold value of 0.90×10^{-3} mm^2 · sec^{-1} for minimum ADC, patients with a favorable prognosis were differentiated from those with a poor prognosis according to the best combination of the sensitivity (79%) and specificity (81%).
- The patients with a minimum ADC above this threshold value showed a significantly better prognosis than those with a minimum ADC that was at or below this threshold value.

Materials and Methods

Patients

We reviewed the MR imaging database (X.Y.) from Tohoku University Graduate School of Medicine, Sendai, Miyagi, Japan. From the database, we selected consecutive patients with a pathologic diagnosis of a malignant astrocytic tumor who underwent preoperative MR imaging studies, including isotropic DW imaging, between April 1999 and January 2003 and whose results of clinical follow-up studies were available more than 2 years after their initial treatment. We excluded patients who had undergone a major therapeutic intervention, such as surgery or radiation therapy and chemotherapy, before initial MR imaging with DW imaging. Thirty-seven patients met the criteria, and the group comprised 21 male and 16 female patients who were 7–75 years in age (mean, 43 years). The ethics committee of Tohoku University Hospital, Tohoku, Japan, approved this retrospective study and did not require patient informed consent. Medical records, pathologic reports, surgical notes, and results of all MR imaging studies for all the patients were available. Pretreatment performance status of the patients was evaluated according to the Eastern Cooperative Oncology Group score, which ranges from 0 to 5, with 0 denoting perfect health and 5 denoting death (16).

Pathologic Evaluation and Surgery

The pathologic diagnosis included 22 GBMs and 15 anaplastic astrocytomas (AAs). The diagnosis was determined with specimens removed at surgical resection or biopsy, according to the World Health Organization criteria, by a neuropathologist (M.W.) with 15 years of experience. The specimens were obtained from both enhanced and nonenhanced areas of each tumor with

Published online before print
10.1148/radiol.2413051276

Radiology 2006; 241:839–846

Abbreviations:
AA = anaplastic astrocytoma
ADC = apparent diffusion coefficient
DW = diffusion weighted
GBM = glioblastoma
LI = labeling index

Author contributions:
Guarantors of integrity of entire study, S.H., X.Y.; study concepts/study design or data acquisition or data analysis/interpretation, all authors; manuscript drafting or manuscript revision for important intellectual content, all authors; manuscript final version approval, all authors; literature research, S.H., X.Y., T.K., S.M., A.U., T.Y.; clinical studies, T.K., M.W.; statistical analysis, S.H., X.Y., S.M., A.U., A.S., S.T.; and manuscript editing, S.H., X.Y., T.K., M.W., S.M., A.S., T.Y., S.T.

Authors stated no financial relationship to disclose.

reference to three-dimensional contrast material–enhanced MR images by using a neuronavigational system (ViewScope; Elekta IGS, Grenoble, France) during surgery or biopsy. In addition to the conventional histopathologic evaluation, the Ki-67 LI was retrospectively determined in 36 patients (M.W.). In this process, fields with the highest number of Ki-67–labeled cells were initially selected through a generalized survey, and then a percentage of positively labeled cells was determined by counting more than 1000 tumor nuclei at ×400 magnification.

Surgical removal was undertaken in 30 patients, whereas stereotactic biopsy was performed in seven patients, and these patients included one with GBM and six with AAs. All of the procedures were performed by one neurosurgeon (T.K.) with 18 years of experience. With surgical removal, we intended to remove the maximum amount of tumor, which included nonenhanced portions of lesions and enhanced lesions, with minimum neurologic, physical, and systemic damage by using a neuronavigational system and intraoperative neurophysiologic mapping techniques. In 28 tumors, almost all of the tumor—a portion that included the entire enhanced components—was removed. For the other two tumors, some of the enhanced portions partially remained in place. Two neuroradiologists (S.H. and X.Y., with 20 and 3 years of experience, respectively) performed those determinations in consensus by comparing preoperative MR images with postoperative initial ones obtained within 1 week after the surgical intervention. The stereotactic biopsy was performed only in cases with a tumor that involved the brainstem (n = 3) or in those with a tumor that was extensively infiltrating the cerebral hemisphere and included eloquent areas such as the primary motor cortex, the pyramidal tract, or speech (Broca) areas (n = 4).

Postoperative Treatment and Follow-up

After surgery, all the patients subsequently received radiation therapy according to the protocol of our hospital. For AAs, local brain irradiation of 72 Gy for 30 days (5 days a week for 6 weeks) was delivered with the hyperfractionation method (1.2 Gy delivered twice a day). For GBM, whole-brain irradiation of 30 Gy for 15 days (5 days a week for 3 weeks) was delivered with the conventional method, and afterward, localized irradiation of 30 Gy for 10 days (5 days a week for 2 weeks) was delivered with the accelerated hyperfractionation method (1.5 Gy delivered twice a day). All the patients were evaluated at monthly outpatient examinations, and head MR imaging was performed every 2 months. For chemotherapy, 1-(4-amino-2-methyl-5-pyrimidinyl)-methyl-3-(2-chloroethyl)-3-nitrosourea, also called ACNU, was administered every 2 months for 2 years.

Observing these patients for 2 years after the initial treatment, we (S.H., X.Y.) classified them into stable and progressive groups according to their clinical courses and follow-up MR imaging findings. The stable group consisted of the patients who were alive and in whom additional enhanced lesions were not revealed at MR imaging, with the exception of transient contrast enhancement along the margin of resection cavities related to surgical intervention. In the patients of this group, the clinical status also remained stable and the residual tumors, including the nonenhanced portions, if any, showed no obvious change on follow-up MR images. The progressive group included patients who died of progression of the brain disease related to their tumors and those who developed pathologically proved recurrent tumors or obvious enhanced lesions suggestive of tumor recurrence and/or dissemination that were revealed at MR imaging. Although this classification was based on the status at 2 years after the initial treatments, the patients were followed up until January 2005 if they were available for evaluation of the prognosis.

MR Imaging and Data Processing

The patients were imaged by using a 1.5-T MR imaging system (Signa Horizon LX CV/i; GE Medical Systems, Milwaukee, Wis) and a conventional quadrature head coil. The contrast agent was gadopentetate dimeglumine (Magnevist; Nihon Schering, Osaka, Japan) or gadodiamide injection (Omniscan; Daiichi Pharmaceuticals, Tokyo, Japan). Nonenhanced and contrast-enhanced T1-weighted MR images, T2-weighted MR images, and DW images were obtained during the same imaging session without repositioning each patient's head. DW imaging was performed by using fat-suppressed spin-echo echo-planar imaging (repetition time msec/echo time msec, 5000/72; number of signals acquired, two; section thickness, 6 mm; gap, 2 mm; matrix, 128 × 128; field of view, 23 × 23 cm) with three orthogonal directional motion-probing gradients (b = 1000 sec/mm^2), followed by automatic generation of isotropic DW images. Images without motion-probing gradients (b = 0 sec/mm^2) were simultaneously obtained as well. The interval between the preoperative MR imaging studies and the surgery was shorter than 1 month (mean, 12 days). All the patients additionally underwent three-dimensional contrast-enhanced imaging with the neuronavigational system fewer than 3 days before surgery, and no substantial difference was noted in imaging findings between MR imaging studies with DW imaging and MR imaging studies with the neuronavigational system.

ADC maps were calculated from isotropic DW images and images obtained with a b value of 0 sec/mm^2 by using standard software with a different workstation (Dr. View Pro 5.3; Ashahi Information System, Tokyo, Japan). The minimum ADC value of each tumor was determined by placing regions of interest by using the same workstation as was used to generate ADC maps in the following procedures (S.H.). We at first selected all continuous sections that included tumor. Several round- or oval-shaped regions of interest (area, approximately 0.3 cm^2, 10 pixels) were carefully placed on each selected section of the ADC map to include the area with the lowest ADC value determined with visual inspection, preferably with avoidance of cystic, necrotic, or hemorrhagic

components of the tumor with reference to conventional MR images. Finally, a value of a region of interest with the lowest ADC value was chosen from these regions of interest as a minimum ADC value of the tumor.

Statistical Analysis

The relationship between minimum ADC and Ki-67 LI was analyzed by using correlational analysis (Pearson product moment correlation). In comparing every parameter between two groups (AA and GBM groups, stable and progressive groups), equality of variances was evaluated by using the F test to select statistical tests. The minimum ADC values, with variances that were homoscedastic, were analyzed with the Student t test. The Welch test was applied to the analysis of the Ki-67 LI, patient age, and performance status because the variances of these parameters were not homoscedastic. A P value of less than .05 was considered to indicate a statistically significant difference. These statistical analyses were performed (S.H., S.M.) by using software (StatView 5.0, 1998; SAS Institute, Cary, NC).

A receiver operating characteristic analysis was applied to assess which cutoff value of minimum ADC had the best combination of sensitivity and specificity to allow differentiation of the stable group from the progressive group. The selection of the critical cutoff point varies with a trade-off between sensitivity and specificity. We considered a value that maximized the sum of sensitivity and specificity as the best cutoff point. The fitted receiver operating characteristic curve was constructed with software (ROCKIT, version 0.9.1b, 1998; *http://xray.bsd.uchicago.edu/krl/KRL_ROC/software_index.htm#ROCKIT*).

To compare the prognosis of the two groups classified according to the cutoff value of minimum ADC determined with the analysis mentioned previously, the Kaplan-Meier method and log-rank test were applied by using software (StatView 5.0). In this analysis, the event time was calculated as the following: For the patients who died of tumor progression or who had recurrent tumors, the time between the date of the initial surgery and that of death or recurrence was defined as the event time. The stable patients were censored at the last available follow-up date.

Results

Ki-67 LI and Minimum ADC

Although no significant correlation between Ki-67 LI and minimum ADC was noted for the AA group ($r = -0.416$, $P = .12$) or the GBM group ($r = -0.253$, $P = .27$) separately, there was a significant negative correlation between these parameters for the malignant astrocytic tumors as a whole ($r = -0.562$, $P < .001$) (Fig 1). In regard to patient age, pretreatment performance status, minimum ADC value, and Ki-67 LI, compared between AA and GBM groups (Table 1), the mean minimum ADC value for the GBM group was significantly lower than that for the AA group, and there was overlap between the values for the two groups (Figs 1, 2). The mean value of Ki-67 LI also was significantly different between these two groups.

Figure 1

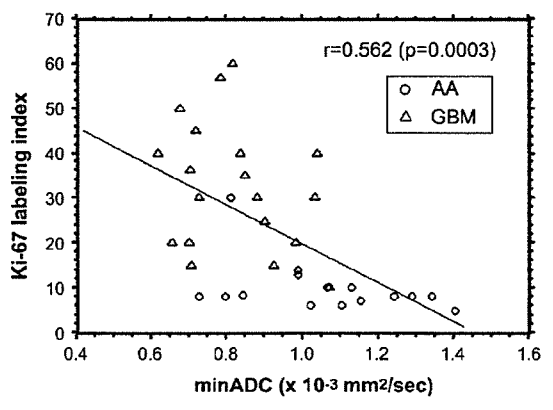

Figure 1: Graph shows relationship between minimum ADC and Ki-67 LI. Significant negative correlation was noted between these parameters for astrocytic tumors as a whole. GBMs generally show higher Ki-67 LI and lower minimum ADC, whereas AAs show lower Ki-67 LI and higher minimum ADC.

Table 1

Comparison of Patient Age, Pretreatment Performance Status, Minimum ADC Value, and Ki-67 LI for GBM and AA Groups

Parameter	GBM Group ($n = 22$)*	AA Group ($n = 15$)	P Value†
Age (y)	46.6 ± 18.5 (7–75)	41.6 ± 14.2 (23–64)	.42‡
Performance status	1.1 ± 1.1 (0–3)	0.6 ± 1.1 (0–4)	.25‡
Minimum ADC ($\times 10^{-3}$ mm^2 · sec^{-1})	0.834 ± 0.136 (0.616–1.073)	1.060 ± 0.207 (0.726–1.402)	<.001
Ki-67 LI (%)	33.2 ± 13.8 (10–60)	9.96 ± 6.06 (5–30)	<.001

Note.—Values are the mean ± standard deviation, and numbers in parentheses are ranges.

* Ki-67 LI was available in 21 patients in the GBM group.

† The minimum ADC value was analyzed with the Student t test, and age, performance status, and Ki-67 LI were analyzed with the Welch test.

‡ Not significant.

Figure 2

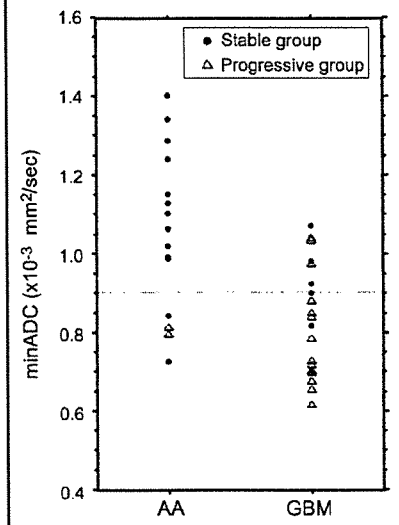

Figure 2: Graph shows relationship between minimum ADC and prognosis according to pathologic type. Minimum ADC values of AAs are higher than those of GBMs, although substantial overlap is noted. With the cutoff value of 0.90×10^{-3} $mm^2 \cdot sec^{-1}$ for minimum ADC, most of the patients in the stable group have values above this threshold, and most of the patients in the progressive group have values below that level.

Figure 3

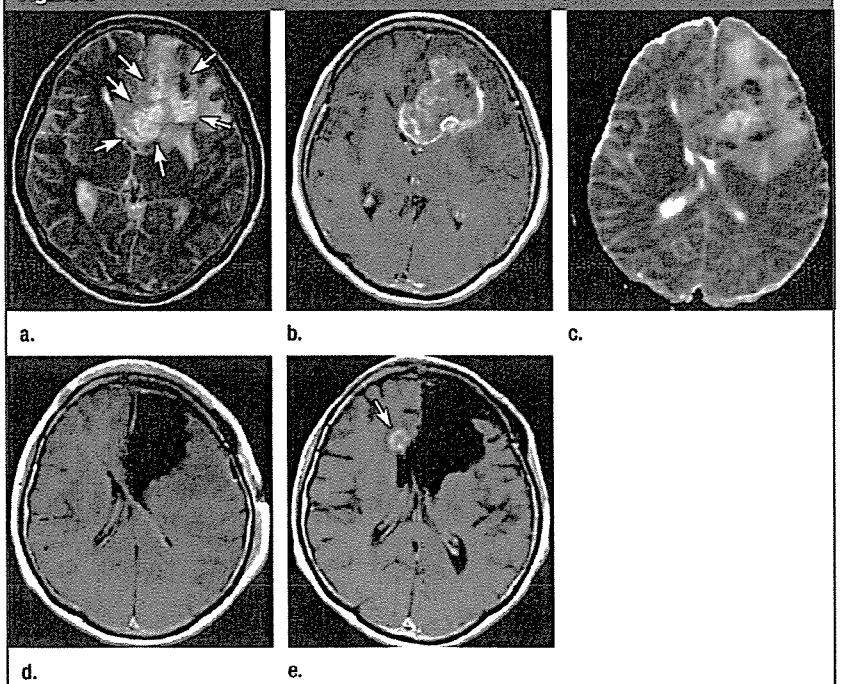

Figure 3: GBM in 56-year-old woman. Transverse **(a)** preoperative T2-weighted MR image (3600/96), **(b)** contrast-enhanced T1-weighted MR image (440/14), and **(c)** ADC map show irregularly shaped enhancing tumor (arrows in a) with perifocal edema in left mediofrontal lobe. Minimum ADC value was 0.72×10^{-3} $mm^2 \cdot sec^{-1}$. **(d)** Postoperative contrast-enhanced transverse T1-weighted MR image (440/14) shows gross total removal of the tumor. **(e)** Contrast-enhanced transverse T1-weighted MR image (440/14) 9 months after surgery shows a patchy enhancing lesion (arrow). The lesion enlarged later, and gamma knife therapy was performed. With further progression of the disease, the patient died 1.5 years after initial treatment.

Follow-up

From the results of 2-year follow-up after the initial treatment, 19 patients (13 with AAs and six with GBMs) were classified as the stable group, and 16 patients (two with AAs and 14 with GBMs) were classified as the progressive group (Figs 3, 4). In the latter group, 13 patients (11 with GBMs, two with AAs) died of exacerbation of the brain tumors within the observation period, whereas in the remaining three patients with GBMs, recurrent tumors developed (pathologically proved at repeat surgery). Two patients with GBMs were excluded from this classification because they died of pneumonia within 2 years despite no clinical evidence of tumor recurrence. Therefore, the following analysis was performed by using 35 patients without these two patients.

There was a significant difference in mean values of minimum ADC and Ki-67 LI between the stable and progressive groups (Table 2). All except two patients with AAs belonged to the stable group and had relatively higher minimum ADC values (Fig 2). The remaining two patients with AAs had a poor prognosis and relatively low minimum ADC values. Six patients with GBMs belonged to the stable group, and four of them had relatively higher minimum ADC values.

According to the receiver operating characteristic analysis (Fig 5), the cutoff value of 0.90×10^{-3} $mm^2 \cdot sec^{-1}$ in minimum ADC generated the best combination of sensitivity (79%) and specificity (81%). Receiver operating characteristic analysis of patients with removal of almost the entire tumor yielded similar results (area under the receiver operating characteristic curve, 0.83), with sensitivity of 87% and specificity of 73% by using the same cutoff value.

When the prognosis was compared between the two groups classified by using the previously mentioned cutoff value of minimum ADC (0.90×10^{-3} $mm^2 \cdot sec^{-1}$) and the Kaplan-Meier method, the group with the higher minimum ADC showed significantly better outcome ($P = .002$, log-rank test) (Fig 6). If the same analysis was applied to other sets of pairs classified by using different cutoff values, namely 0.80×10^{-3} $mm^2 \cdot sec^{-1}$ and 1.00×10^{-3} $mm^2 \cdot sec^{-1}$, the P values achieved with the log-rank test were .01 and .1, respectively.

Discussion

We found a significant negative relationship between minimum ADC and Ki-67 LI for the malignant astrocytic tumors in general, although no significant correlation was noted for the AA group or the

GBM group separately. Few reports have been published in which a direct comparison of ADC values with the Ki-67 LI was performed. Calvar et al (17) reported a significant inverse correlation between ADC values and Ki-67 LI in their analysis of 37 brain tumors with various pathologic findings. Findings in many studies (7,8,11,14,15), however, suggest that ADC values are inversely correlated and the choline signal at proton MR spectroscopy is positively correlated with tumor cell density in various kinds of brain tumors. Findings in several reports indicate that there is an inverse correlation between ADC values and choline signal in gliomas at MR spectroscopy (7,8).

In an MR spectroscopic study of astrocytomas, Tamiya et al found that the choline-creatine ratio correlated positively with Ki-67 LI and that the *N*-acetylaspartate–choline ratio correlated inversely with Ki-67 LI, and they suggested that the choline signal at MR spectroscopy should reflect cellular proliferation (18). Considering all these results together, it is understandable that the ADC values correlated with the

Figure 4

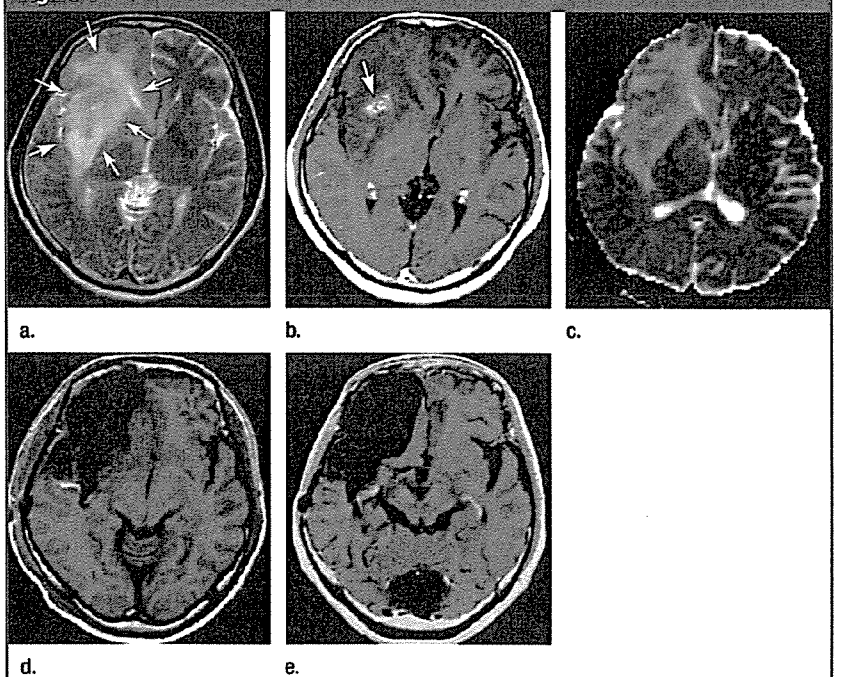

Figure 4: GBM in 43-year-old man. Transverse **(a)** preoperative T2-weighted MR image (3600/96), **(b)** contrast-enhanced T1-weighted MR image (440/14), and **(c)** ADC map show ill-defined tumor (arrows in **a**) in right insulo-opercular region. Irregular enhancing area is noted in center of tumor (arrow in **b**). Minimum ADC value was 1.07×10^{-3} mm^2 · sec^{-1}. **(d)** Postoperative contrast-enhanced transverse T1-weighted MR image (440/14) shows that most of the tumor, including all enhancing components, was removed. **(e)** Contrast-enhanced transverse T1-weighted MR image (440/14) 2 years after surgery shows no tumor recurrence.

Figure 5

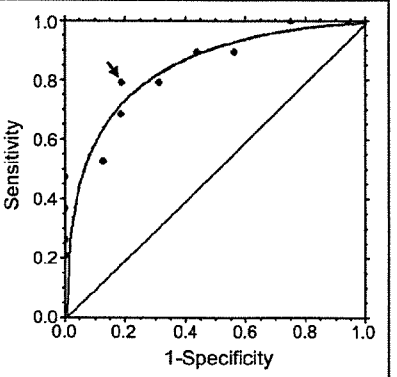

Figure 5: Empiric and fitted receiver operating characteristic curves of minimum ADC values for use in differentiation of stable patients from progressive patients. Area under the receiver operating characteristic curve was 0.854. When the minimum ADC is 0.90×10^{-3} mm^2 · sec^{-1}, the best combination of sensitivity (79%) and specificity (81%) is provided (arrow).

Table 2

Comparison of Patient Age, Pretreatment Performance Status, Minimum ADC Value, and Ki-67 LI for Stable and Progressive Groups

Parameter	Stable Group (n = 19)	Progressive Group (n = 16)*	P Value†
Age (y)	42.0 ± 11.9 (23–64)	44.3 ± 20.0 (7–67)	.53‡
Performance status	0.6 ± 1.2 (0–4)	0.9 ± 0.9 (0–2)	.49‡
Minimum ADC ($\times 10^{-3}$ mm^2 · sec^{-1})	1.037 ± 0.196 (0.705–1.402)	0.800 ± 0.131 (0.616–1.039)	<.001
Ki-67 LI (%)	13.5 ± 12.3 (5–60)	34.1 ± 12.4 (8–56.7)	<.001

Note.—Values are the mean ± standard deviation, and numbers in parentheses are ranges.

* Ki-67 LI was available in 15 patients in the progressive group.

† The minimum ADC value was analyzed with the Student *t* test, and age, performance status, and Ki-67 LI were analyzed with the Welch test.

‡ Not significant.

Ki-67 LI. It is likely that tumors with high proliferation activity (high Ki-67 LI) should have potency of rapid growth, yielding high cellularity. Kiss et al histopathologically assessed cell density and Ki-67 LI in 54 astrocytic tumors and found a significant correlation between them (3).

Because our study was retrospective, the regions for measuring the minimum ADC did not exactly correspond to those for the Ki-67 LI. This might be one reason why the significant correlation was not noted for AA and GBM groups separately, because these gliomas are often very heterogeneous. The following discussion, however, may justify the meaning of the significant relationship between these parameters in all cases. The Ki-67 LI, which was obtained from the fields packed most closely with labeled cells, should have reflected the value from one of the regions with the highest cell density in the specimen. Similarly, the minimum ADC value should represent the value of the region with the highest cellularity of each tumor.

There was a significant difference in the mean minimum ADC values between the AA and GBM groups. In many studies (9,10,14) about the assignment of grades to gliomas, researchers found a significant difference in tumor ADC values between low-grade (World Health Organization grades I and II) and high-grade (World Health Organization grades III and IV) gliomas and/or metastases. As far as we know, however, no investigators observed a significant difference in ADC between high-grade gliomas, that is, AA (grade III) and GBM (grade IV). Most investigators evaluated diffusional properties in various pathologic types of tumors altogether rather than in a single type of tumor. Because the tumor cell density would be inherently different in each pathologic type, the same World Health Organization grade of different kinds of tumors may vary in regard to their cell density. We compared ADC values that focused on malignant astrocytic tumors (AA and GBM), which might have resulted in a significant difference. The overlap in minimum ADC values of each group, however, was so large that the differentiation between them could not be based solely on the value of the minimum ADC.

Figure 6

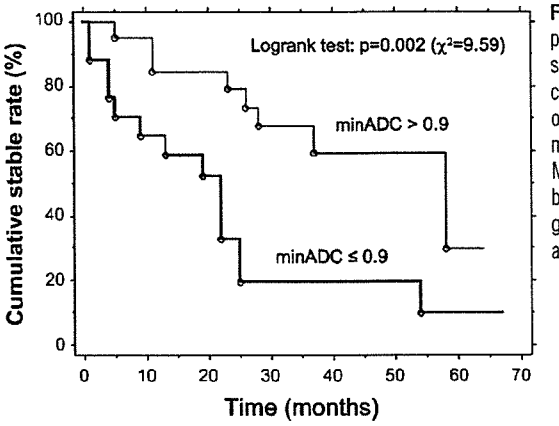

Figure 6: Graph shows comparison of postoperative prognosis between two groups of patients classified according to cutoff value of 0.90×10^{-3} mm^2 · sec^{-1} for minimum ADC by using Kaplan-Meier method. The significantly better outcome was noted in the group with a minimum ADC value above the cutoff value.

The mean minimum ADC value of the stable group was significantly higher than that of the progressive group. A significant difference in Ki-67 LI was also found between these two groups. Several investigators (3,5,6) have revealed the prognostic importance of Ki-67 LI in astrocytic tumors. Kiss et al (3) observed that there was a marked difference in survival periods between the patients with a tumor that exhibited a low level of Ki-67 LI and low cell density and those with a tumor that exhibited a high level of Ki-67 LI and high cell density. Torp (5) found that Ki-67 LI increased significantly with increasing malignancy grade of astrocytomas and that tumors with the higher Ki-67 LI had significantly poorer prognosis than those with lower indexes. Neder et al (6) also reported a close relationship between MIB-1 LI (equivalent to Ki-67 LI) and survival of patients with astrocytomas.

Such an index, however, is measurable only after harvesting samples of tumor specimens. We could not find any published reports that indicated the usefulness of preoperative assessment of tumor ADC for prediction of posttherapeutic prognosis. Oh et al (19) investigated the relationship between ADC values and survival time in patients with GBM. They compared ADC values after surgery but prior to radiation therapy with patient survival times, and they showed that there was a significantly shorter median survival time in patients with low ADC compared with that in patients with high ADC within the residual region of T2 elongation.

In the present study, the prognosis of each tumor after initial treatments (surgery or radiation therapy and chemotherapy) could be well predicted by using preoperative measurement of the minimum ADC of the tumor. The threshold values of 0.90×10^{-3} mm^2 · sec^{-1}) in minimum ADC provided the best combination of sensitivity and specificity for prediction of prognosis. Actually, when we compared the prognosis between the two groups classified by using this threshold, the group with the higher minimum ADC had a significantly better outcome. When we considered the result that indicated a significant correlation between minimum ADC and Ki-67 LI, it was not surprising that tumoral minimum ADC values should have preoperative prognostic importance in patients with a malignant astrocytoma.

Stereotactic biopsy often is performed to establish a diagnosis in patients with intracranial lesions. As gliomas are typically heterogeneous and can have different histologic grades in a single tumor, the wrong choice of biopsy site may lead to underestimation of a tumor grade, and underestimation may confound determination of the optimum treatment strategy. In such a situation, measurement of minimum ADC may aid in the selection of the appropriate site for the biopsy, because minimum ADC should indicate a